JOURNAL OF MATERIALS SCIENCE 33 (1998) 901–911

Thermal behaviour of a polytitanocarbosilane-derived fibre with a low oxygen content: the Tyranno Lox-E fibre

G. CHOLLON*, B. ALDACOURROU, L. CAPES, R. PAILLER, R. NASLAIN
Laboratoire des composites Thermostructuraux, UMR 47 (CNRS-SEP-UB1), 3, allée de La Boétie, 33600 Pessac, France

The chemical composition, microstructure and mechanical properties of Tyranno Lox-E fibre were studied in the as-received state and after annealing in inert atmosphere. The fibre consists of SiC nanocrystals of 2–3 nm, free carbon aggregates of 4–5 distorted aromatic layers and 1–3 nm in length and an amorphous silicon (titanium) oxycarbide phase. Except for evolution of residual hydrogen and a slight densification, the fibre is chemically and structurally stable and retains a high strength up to 1300 °C. Beyond 1300 °C, superficial degradation resulting from decomposition of the oxycarbide into $SiO_{(g)}$ and $CO_{(g)}$ induces a decrease of strength. Compared with bulk polycrystalline SiC, the fibre has a low creep resistance at high temperature, mainly because of the nanometric size of the SiC crystals but also because of the presence at the grain boundary of the oxycarbide phase (viscous and chemically unstable) and of the poorly organized free carbon phase (chemically and structurally unstable).

1. Introduction

SiC-based fibres, because of their high potential properties, are one of the best candidates for reinforcement of ceramic material composites (CMCs). To reinforce CMCs assigned to high temperature uses, optimized ceramic fibres have to be developed. They must combine high strength, stiffness and creep resistance at high temperatures, have good oxidation resistance as well as low processing costs. SiC-based fibres prepared from organosilicon precursors have been commercialized since the early 1980s [1–4]. They are still one of the most widely used CMCs reinforcements for a temperature use not exceeding 1100–1200 °C. These fibres are not only made of nanocrystalline silicon carbide (having a crystal size of about 2 nm) but also free carbon and amorphous silicon oxycarbide [5–7]. The last phase, especially when combined with free carbon, has a limited thermal stability. It decomposes above 1100–1200 °C into $SiO_{(g)}$ and $CO_{(g)}$ resulting in large SiC grain-coarsening and thus, in a catastrophic decrease of strength [8–14]. Furthermore, with respect to monolithic SiC, these fibres exhibit a limited creep resistance at high temperature still owing to the intergranular amorphous oxycarbide phase [15–18].

It is now well established that the thermal stability of ex-organosilicon precursor fibres can be improved by using an oxygen-free cross-linking process instead of classical oxygen curing, which leads to a much lower oxygen content [19–25]. The aim of the present study is to assess the thermal stability of a new generation SiC-based fibre, i.e. the Tyranno Lox-E fibre. This fibre is probably prepared via the spinning of the same organosilicon precursor, a polytitanocarbosilane (PTCS), as the commercial Tyranno Lox-M fibre (with an oxygen concentration of 18 wt %) but according to an electron beam cross-linking process in the absence of oxygen [25].

2. Experimental procedure

2.1. Materials

The fibres† were provided in the form of a spool of continuous yarn of approximately 500 filaments. They were coated with polyvinyl acetate (PVA), which was removed by a short oxidizing treatment in air (3 min at 600 °C) prior to any analysis.

2.2. Annealing treatments

Annealing treatments were performed with a high-temperature pyrolysis equipment composed of a graphite crucible heated with a radio frequency coil. The samples were rapidly heated (30 °C min^{-1}) and maintained at a given pyrolysis temperature, T_p ($1200 < T_p < 1600$ °C) under a static high-purity argon atmosphere (100 kPa) (Argon N56 from Alphagaz) for a pyrolysis time, t_p, 1 h.

* *Present address*: National Institute of Materials and Chemical Research, 1-1 Higashi, Tsukuba, Ibaraki 305, Japan.
† From UBE Industries, Japan.

2.3. Characterization techniques

Elemental analyses were performed on polished cross-sections by electron probe microanalysis (EPMA) using a Camebax 75 (Cameca) in the wavelength dispersion mode (thallium acid phthalate (TAP) crystal for SiK_α, pentaerytritole (PET) for TiK_α and a multilayer pseudo crystal multilayer (PCII) for CK_α and OK_α) with standards (SiC, Ti and SiO_2) whose compositions were assumed to be stoichiometric. It is worthy of note that the hydrogen content of the samples could not be assessed by EPMA. Chemical analyses of the as-received fibre were also investigated according to conventional procedures.

Auger electron spectroscopy (AES) characterization was performed with a scanning microprobe (PHI 5905 AM, Physical Electronics) equipped with an Ar^+ sputtering gun. The variations of the intensities (peak-to-peak mode) of the Auger electron peaks (LMM-transition for Si and Ti, KLL-transition for C and O) as a function of the sputtering time were used to draw semi-quantitative composition–depth profiles from the surface of the sample (sputtering rate reference: Ta_2O_5).

The morphology of the fibres was studied by scanning electron microscopy (SEM) using an 840 S (Jeol).

The structure of the monofilaments was studied at the nanometre scale by high resolution transmission electron microscopy (TEM) using an EM 400 (Philips). The samples were embedded in an apoxy resin and cut into thin foils with an ultramicrotome. Foils were then set on copper microgrids. The TEM analyses were performed in the bright field (BF), dark field (DF), lattice fringes (LF) and selected area diffraction (SAD) modes.

The X-ray diffraction (XRD) spectra (wavelength, λ, CuK_α) using a D5000 (Siemens) were recorded from a tow of fibres. The apparent mean grain size, L, of the β-SiC crystalline phase present in the samples was calculated from the width, D (in radian), of the (1 1 1) diffraction peak at mid-height, according to the Scherrer equation

$$L = K\lambda/D\cos\theta$$

where K is a constant (taken as one), λ the CuK_α wavelength (i.e. $\lambda = 0.154$ nm) and θ the Bragg angle [$\theta = 17.8^\circ$ for β-SiC (1 1 1)].

Solid state ^{29}Si and ^{13}C nuclear magnetic resonance (NMR) analyses were performed on powder samples for the as-received and the heat treated fibres. The spectra were recorded on spectrometers operating at 99.3 MHz for ^{29}Si (ASX 500, Brucker) and at 25.1 MHz for ^{13}C (ASX 100, Brucker). The samples were spun at 4000–5000 Hz according to the magic angle spinning (MAS) technique.

Neutron diffraction analyses were made on powders with the diffractometer Orphée (Laboratoire Léon Brillouin, Saclay, France). The diffraction patterns display the interference function, $S(q)$, with $q = 4\pi\sin\theta/\lambda$. The pair correlation function, $g(r)$, is calculated from the Fourier transformation of $S(q)$ and shows the oscillating part of the radial distribution function, i.e. the probability to find an atom at a distance, r, from the atom located at the origin.

Electron spin resonance (ESR) experiments were carried out with a Varian X-band spectrometer (10^{10} Hz), at room temperature (295 K). The g-factor, the linewidth, S, and the paramagnetic susceptibility, $\varkappa_p$, were measured. The number of paramagnetic centres, η, was determined using diphenylpicrylhydraxyle (DPPH) as a standard.

The densities of the samples were measured according to helium-pycnometry (Accupyc 1330, Micromeretics) on filament tows.

The thermal stability of the fibres was studied by thermogravimetric analyses (TAG 24, Setaram) under inert atmosphere. Experiments were performed on samples of ~ 100 mg, set in a graphite crucible and progressively heated at a rate of $10\,^\circ\mathrm{C\,min^{-1}}$ up to 1800 °C, under flowing high purity argon (pressure, $P = 100$ kPa, gas flow, $Q = 1\,\mathrm{l\,h^{-1}}$).

The monofilaments were tensile tested at room temperature with an apparatus similar to that described by Villeneuve *et al.* [26]. For each T_p condition, a batch of about 20 monofilaments was tested with a gauge length of $L = 25$ mm.

The creep tests at high temperature in argon were carried out on single fibre samples ~ 160 mm in length with a cold grip device. The testing temperature was in the range $1000 < T < 1250\,^\circ$C and the applied stress $0.25 < \sigma < 1$ GPa. The creep apparatus, designed by Bodet *et al.* and the procedure have been described elsewhere [16].

Tensile tests at high temperatures ($T \leqslant 1450\,^\circ$C) in air were also carried out on monofilaments ~ 200 mm in length with a gold grip device. The aim was to characterize the strength and stiffness of the fibres as a function of temperature. Since the duration of the test was short (the fibre was tensile-tested immediately after the testing temperature was achieved, i.e. 1–2 min), oxidation and annealing of the fibres were not supposed to affect the mechanical properties of the fibre strongly.

The high temperature testing apparatus used for the tests was based on the one developed by Villeneuve *et al.* [26]. The procedure is described elsewhere [27].

3. Results and discussion

3.1. Physical and chemical analyses

3.1.1. Bulk chemical analysis

The average compositions of the as-received and annealed fibres obtained by EPMA are shown in Table I. The untreated fibre has a reduced oxygen content (~ 6 at %) with respect to the Tyranno Lox-M fibre (~ 15 at %). This oxygen concentration is nevertheless still significant because it is introduced through the fibre precursor as titanium alkoxide. The chemical analysis also indicates a large carbon excess (~ 23 at %) if one assumes that silicon and titanium are engaged in carbides and/or oxycarbides.

TABLE I Chemical composition (at %) of the Tyranno Lox-E fibre

Si	C	O	Ti	C/Si	Free C
36.0	57.0	6.0	0.9	1.58	23.2

The bulk composition of the annealed fibre is stable up to $T_p = 1500\,^{\circ}C$ for $t_p = 1$ h. For $T_p = 1600\,^{\circ}C$ and $t_p = 1$ h, a scale resulting from decomposition ($\sim 1\,\mu m$ in thickness) at the surface of the fibre was observed by optical microscopy and SEM. An attempt to analyse this scale was made and showed a significant decrease of the oxygen content of the decomposed material. This phenomenon is commonly encountered for oxygen-cured organosilicon precursor-based fibres [28, 29]. It is due to the decomposition resulting from the oxygen depletion of the outer part of the fibre (and subsequently extending to the core), according to a "skin–core" effect.

3.1.2. Surface chemical analysis

The depth concentration profile of the untreated fibre, as determined by AES is shown in Fig. 1. The composition of the surface is close to that of the core except for a thin oxygen- and carbon-enriched layer of about 10 nm thickness. The AES analysis of the fibre after erosion of this oxygen-enriched layer is in good agreement with the one obtained by EPMA.

The concentration profile recorded for the fibre treated at $T_p = 1200\,^{\circ}C$ is nearly the same as that of the untreated fibre. Conversely, from $T_p = 1300\,^{\circ}C$, the oxygen concentration at the surface of the fibre drastically decreases, at least along the thickness of the analysed depth. For $T_p = 1400\,^{\circ}C$, the oxygen concentration at the surface of the fibre has almost vanished and a silicon-depleted layer (~ 100 nm in thickness) is also observed. The superficial degradation starting at $T_p = 1300\,^{\circ}C$ and extending at $T_p = 1400\,^{\circ}C$ is a preliminary effect of the decomposition of the fibre, previously revealed by the bulk analyses for $T_p = 1600\,^{\circ}C$.

3.1.3. Morphological analysis

The surface of the untreated fibre is smooth and its fracture surface is typical of a vitreous material (Fig. 2a). From $T_p = 1300\,^{\circ}C$, small crystals are observed at the surface of the fibre (of several tens of nanometres, Fig. 2b). Additionally, the bulk microstructure of the fibre displays a higher crystallization state (Fig. 2c). A larger coarsening of the grains is observed at the surface of the fibre at a higher temperature ($T_p = 1400\,^{\circ}C$, Fig. 2d). The formation of SiC crystals at the surface of the fibre results from the reaction of the gaseous species, $SiO_{(g)}$ and $CO_{(g)}$, generated by the superficial decomposition of the fibre. This feature has been extensively described in studies concerning the thermal behaviour of oxygen-cured organosilicon precursor-based fibres [8–11, 28].

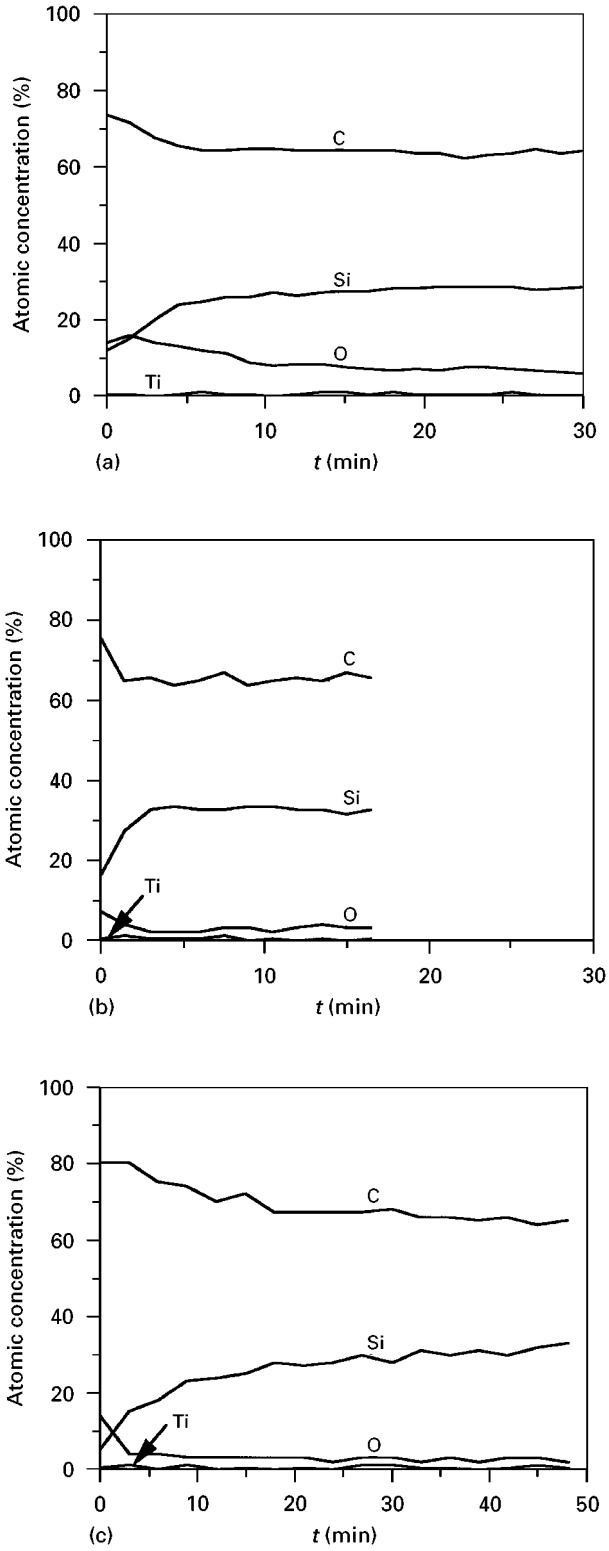

Figure 1 AES depth concentration profile of the surface of the Tyranno Lox-E fibre annealed for 1 h in argon: (a) $T_p = 1200\,^{\circ}C$, (b) $T_p = 1300\,^{\circ}C$, and (c) $T_p = 1400\,^{\circ}C$ (sputtering rate, 2.7 nm min^{-1}; reference standard, Ta_2O_5).

3.1.4. TEM analysis

β-SiC and free carbon phases whose presence was suggested by chemical analyses are both observed by TEM. The largest SiC crystals are approximately 3–4 nm in size and the carbon aggregates are about 1–3 nm in length, L_a, and consist of a maximum of four–five distorted turbostratic layers (Fig. 3a, b) [30]. No gradient nor preferential orientation of either phases were evidenced.

The SiC grain size increases after annealing at $T_p = 1400\,^{\circ}C$. It reaches a maximal size of about 15 nm (Fig. 4a). The free carbon phase, which was hardly seen in the as-processed fibres because of its too low organization state, is better organized for $T_p = 1400\,^{\circ}C$ and appears to be abundant (Fig. 4b).

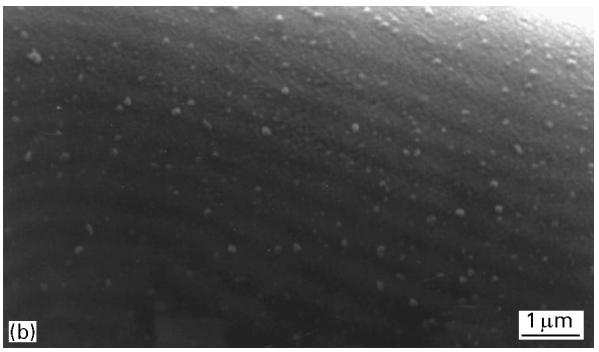

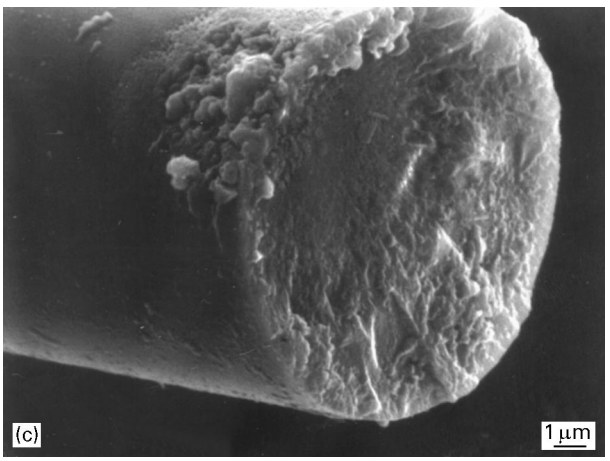

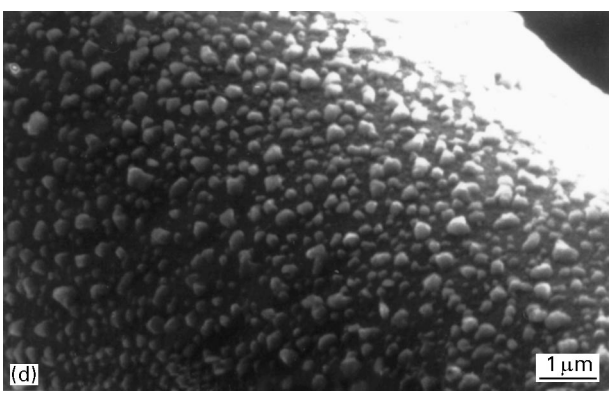

Figure 2 Tyranno Lox-E fibre: (a) fracture surface, (b) the surface of the fibre annealed for 1 h at 1300 °C under argon, (c) the fracture surface of the fibre annealed for 1 h at 1300 °C under argon, and (d) the surface of the fibre annealed for 1 h at 1400 °C under argon.

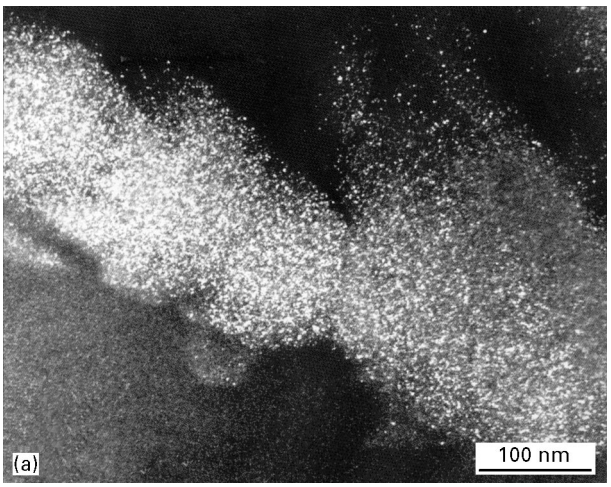

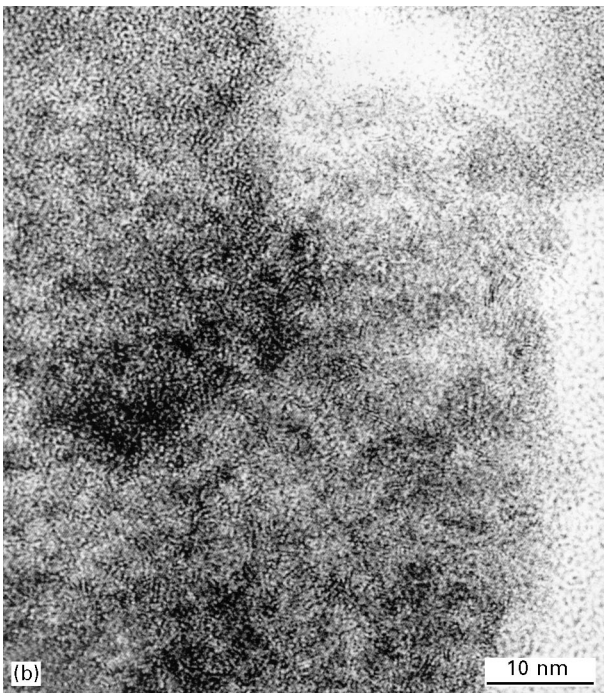

Figure 3 The Tyranno Lox-E fibre: (a) SiC-1 1 1 dark field image and (b) lattice fringe image.

The number of stacked aromatic layers in the carbon aggregates is almost unchanged for $T_p = 1400\,^{\circ}C$, but their grains are slightly greater in size ($L_a = 2$–4 nm) although they are still distorted.

3.1.5. XRD analysis

The XRD spectra recorded for the as-received and annealed fibres show three main peaks corresponding to the (1 1 1), (2 2 0) and (3 1 1) reflections for β-SiC, respectively at $2\theta = 35.8$, 60.0 and 72.1° (Fig. 5). The crystal size, calculated from the Scherrer equation is plotted versus T_p in Fig. 6. The average grain size is 2.2 nm for the as-received fibre, in good agreement with the TEM analyses.

A slight increase of the average grain size of SiC is observed from $T_p = 1200\,^{\circ}C$ and is strongly activated by higher T_p values. The grain size reaches 7.5 nm for $T_p = 1500\,^{\circ}C$.

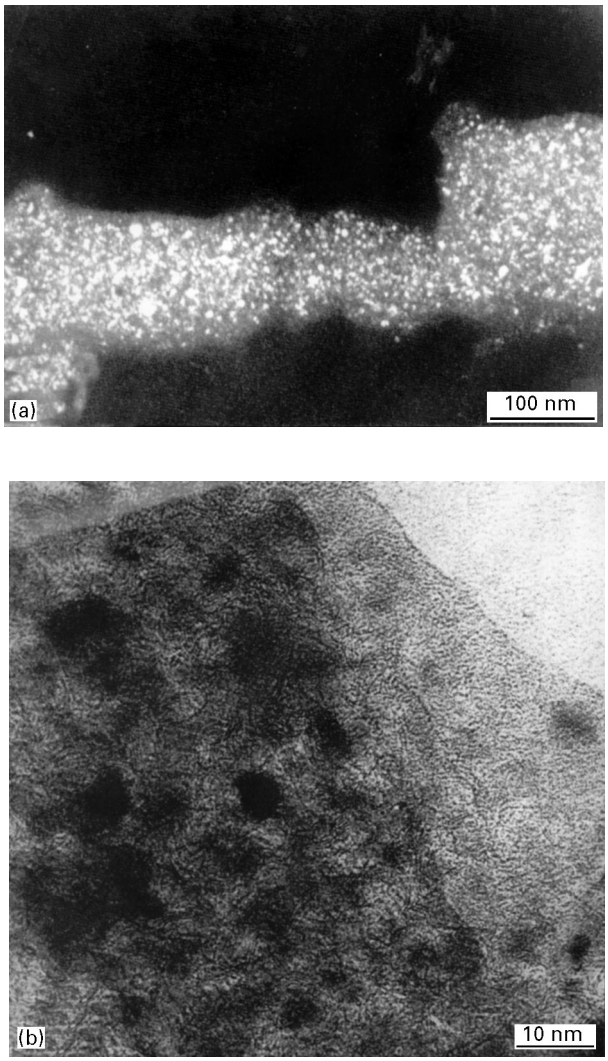

Figure 4 The Tyranno Lox-E fibre annealed for 1 h in argon at $T_p = 1400\,^{\circ}C$: (a) SiC-1 1 1 dark field image and (b) lattice fringe image.

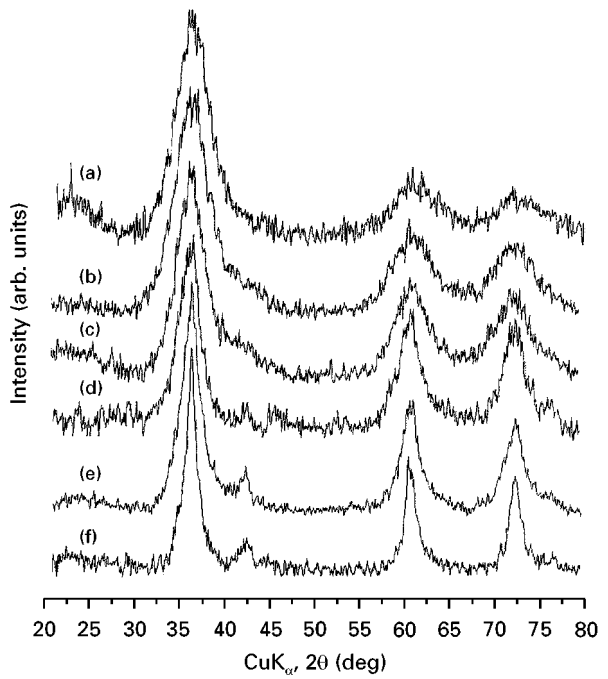

Figure 5 XRD patterns of the Tyranno Lox-E fibre, as-received and annealed for 1 h in argon: (a) as-received, (b) $T_p = 1100\,^{\circ}C$, (c) $T_p = 1200\,^{\circ}C$, (d) $T_p = 1350\,^{\circ}C$, (e) $T_p = 1400\,^{\circ}C$, and (f) $T_p = 1500\,^{\circ}C$.

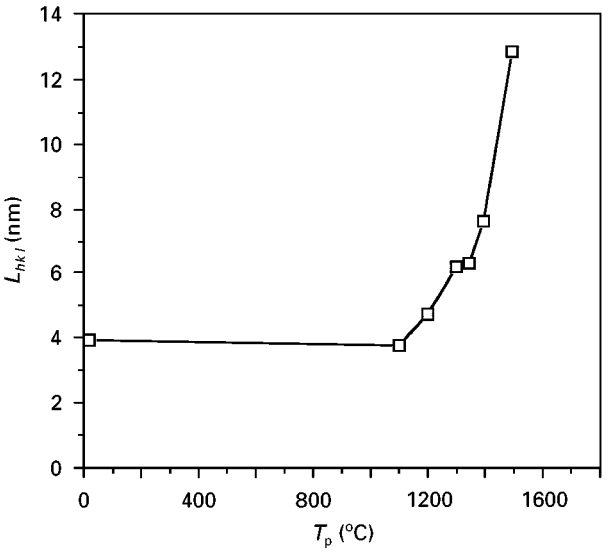

Figure 6 Evolution of the average SiC grain size of the Tyranno Lox-E fibre versus the annealing temperature in argon ($t_p = 1$ h, $P = 100$ kPa).

While large superficial SiC-coarsening is due to the reaction of vapour species, SiC-grain growth of the bulk (observed by TEM analysis) without any chemical change (hydrogen excepted) might involve an atomic or molecular diffusion mechanism through the intergranular material [31].

3.1.6. Solid state NMR analysis

The ^{29}Si–MAS–NMR spectrum of the as-received Tyranno Lox-E fibre shows an intense and broad band centred at -16 p.p.m. and a very weak band at -80 p.p.m. (Fig. 7a). As a matter of fact, the peak at -16 p.p.m. might be decomposed into three bands centred at 0, -16 and -35 p.p.m., the latter being observable under the form of a shouldering of the -16 p.p.m. peak. These bands are assigned to the different tetrahedral environments of silicon: Si–C_4 (-16 p.p.m.), Si–C_3O (0 p.p.m.), Si–C_2O_2 (-35 p.p.m.) and Si–CO_3 (-75 p.p.m.) [5].

The ^{13}C-MAS-NMR spectrum shows two broad bands at 20 and 130 p.p.m., respectively, assigned to the C–Si_4 tetrahedral structure (C sp^3) and the graphite-like polyaromatic structure (C sp^2) (Fig. 7b). These features confirm the prevalence of the SiC phase as well as the presence of free carbon (as assessed by TEM) and of an oxycarbide phase SiO_xC_y that is, at the sight of the relative NMR-peak intensities, less abundant than for the Nicalon NL200 fibre.

3.1.7. Neutron diffraction analysis

The raw diffraction diagram, $S(q)$, for the as-received fibre clearly shows a fall of the background (Fig. 8a). This feature is usually related to residual hydrogen in the material [32]. The hydrogen atoms induce a decreasing shape coefficient of $S(q)$. This decreasing background is no longer observed for the fibre annealed for 1 h at $T_p = 1400\,^{\circ}C$. The heat treatment may result in the vanishing of hydrogen atoms of the

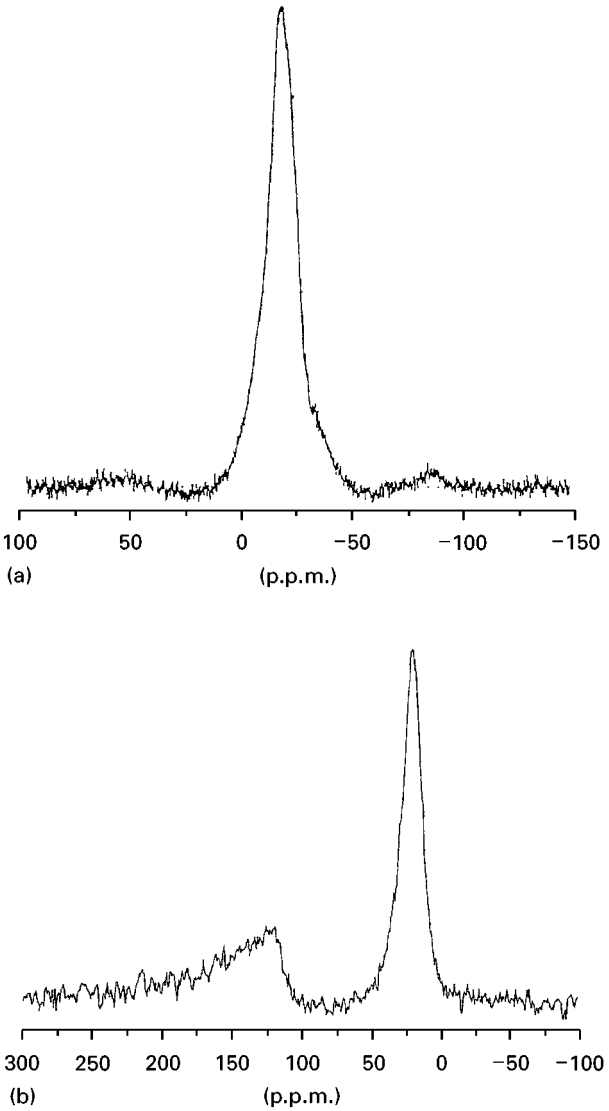

Figure 7 MAS–NMR spectra of the Tyranno Lox-E fibre for (a) ^{29}Si, and (b) ^{13}C.

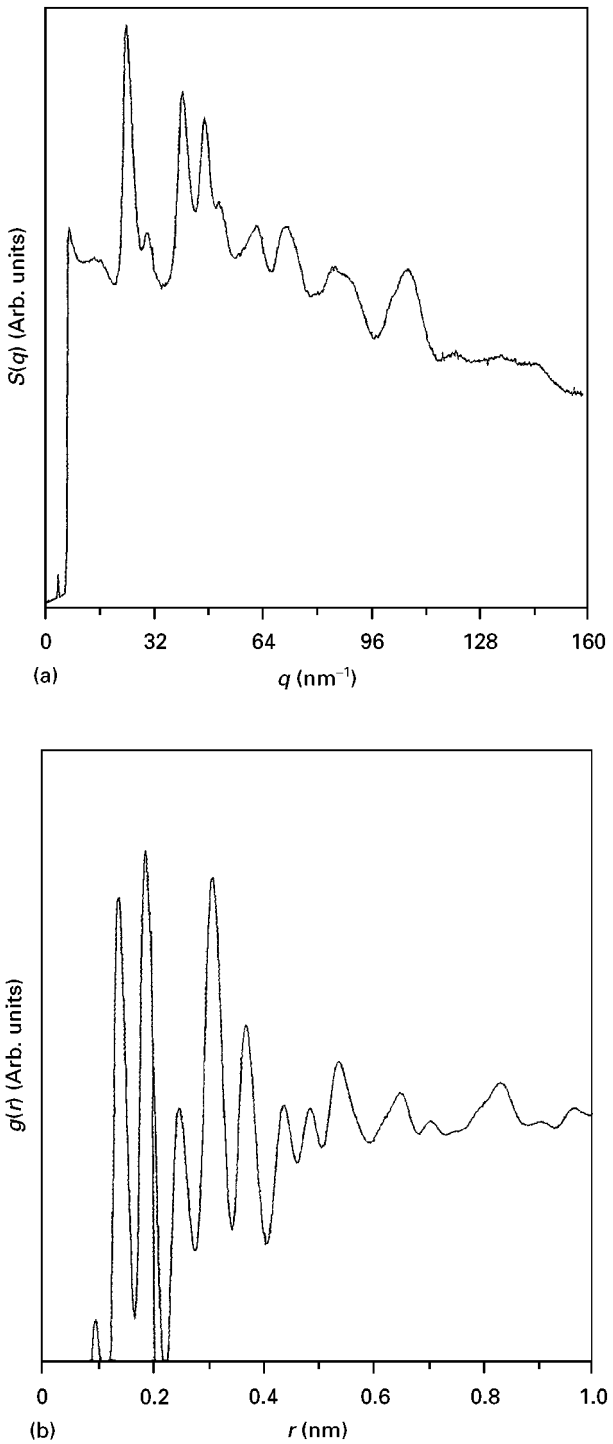

Figure 8 The Tyranno Lox-E fibre: (a) raw neutron diffraction diagram, $S(q)$, and (b) $g(r)$ function diagram.

ceramic, as has already been reported for another organosilicon precursor [32]. The distances measured on the $g(r)$ diagram are characteristic of the graphite-like polyaromatic structure, i.e. theoretically $r = 0.142$ and 0.246 nm for the first and second neighbouring atoms, and for the β-SiC structure, i.e. $r = 0.189$, 0.309, 0.362 and 0.475 nm for the first–fourth neighbouring atoms (Fig. 8b). The distance to the first neighbouring atom of the SiC structure, measured from the fibre is nevertheless slightly lower than the theoretical value (0.187 versus 0.189 nm). This phenomenon might be related to the significant amount of oxygen atoms sharing with carbon the first neighbouring environment of silicon atoms in the SiO_xC_y phase. The Si–O bond ($d = 0.162$ nm) is indeed shorter than the Si–C bond.

TABLE II ESR results for the Tyranno Lox-E fibre

	g	$S(T)$	$\varkappa_p(kg^{-1})$	$\eta(spin\,kg^{-1})$
As-received	2.0026	1.6×10^{-4}	3.52×10^{-5}	1.3×10^{21}
1400 °C for 1 h in Ar	2.0027	1.5×10^{-4}	7.16×10^{-5}	2.7×10^{21}

3.1.8. ESR analysis

ESR data obtained for the as-received and heat-treated fibres ($T_p = 1400$ °C and $t_p = 1$ h) are shown in Table II. The g, S and $\varkappa_p$ values are close to those reported for Si–C–O fibres [33]. From its similarity to that observed for carbon materials, the ESR signal can be assigned to the free carbon phase of the fibre [34, 35]. The paramagnetic susceptibility, $\varkappa_p$, and the spin concentration, η, significantly increase after heat treatment. This feature may correspond to the

elimination of residual hydrogen atoms from the material. As a matter of fact, it is generally admitted that hydrogen in organosilicon-based ceramics is involved in the free carbonaceous phase [36, 37]. Hydrogen atoms are assumed to be bonded to carbon atoms at the edge of the aromatic layers of the aggregates. The rupture of C–H bonds without a full rearrangement may thus result in an increase of the concentration of free radicals, as shown by ESR.

3.1.9. Density measurements

With respect to pure SiC and other SiC-based fibres, the density, ρ, of the as-received fibre is particularly low (Fig. 9). Such a density magnitude is due to the abundant and poorly organized free carbon phase as well as the amorphous SiO_xC_y phase. An increase of the annealing temperature generally results in a densification of the fibres, starting at $T_p = 1100\,^{\circ}C$ and improving at higher temperature. The densification is probably related to the elimination of hydrogen and the ordering of both SiC and free carbon phases that, respectively, occur as the temperature is increased.

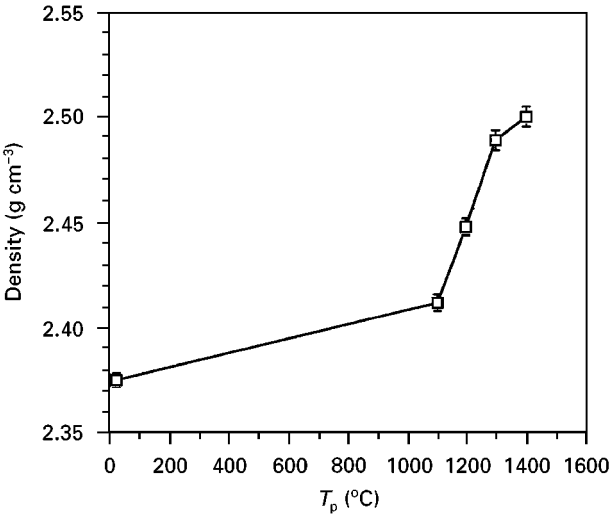

Figure 9 Evolution of the density of the Tyranno Lox-E fibre versus the annealing temperature in argon ($t_p = 1$ h, $P = 100$ kPa).

3.1.10. TGA under inert atmosphere

The variation of the relative weight of the fibre, $\Delta m/m_0$, shows two main steps (Fig. 10). A first slight and graded weight loss occurs from 1050–1100 °C to about $\Delta m/m_0 = -0.43\%$ at 1500 °C. Above this temperature, the relative weight dramatically decreases up to $\Delta m/m_0 = -8\%$ at 1800 °C (for a heating rate of 10 °C min^{-1}). The elimination of hydrogen atoms detected at $T_p = 1400\,^{\circ}C$, but which may start at a temperature as low as 1050 °C, is probably responsible for

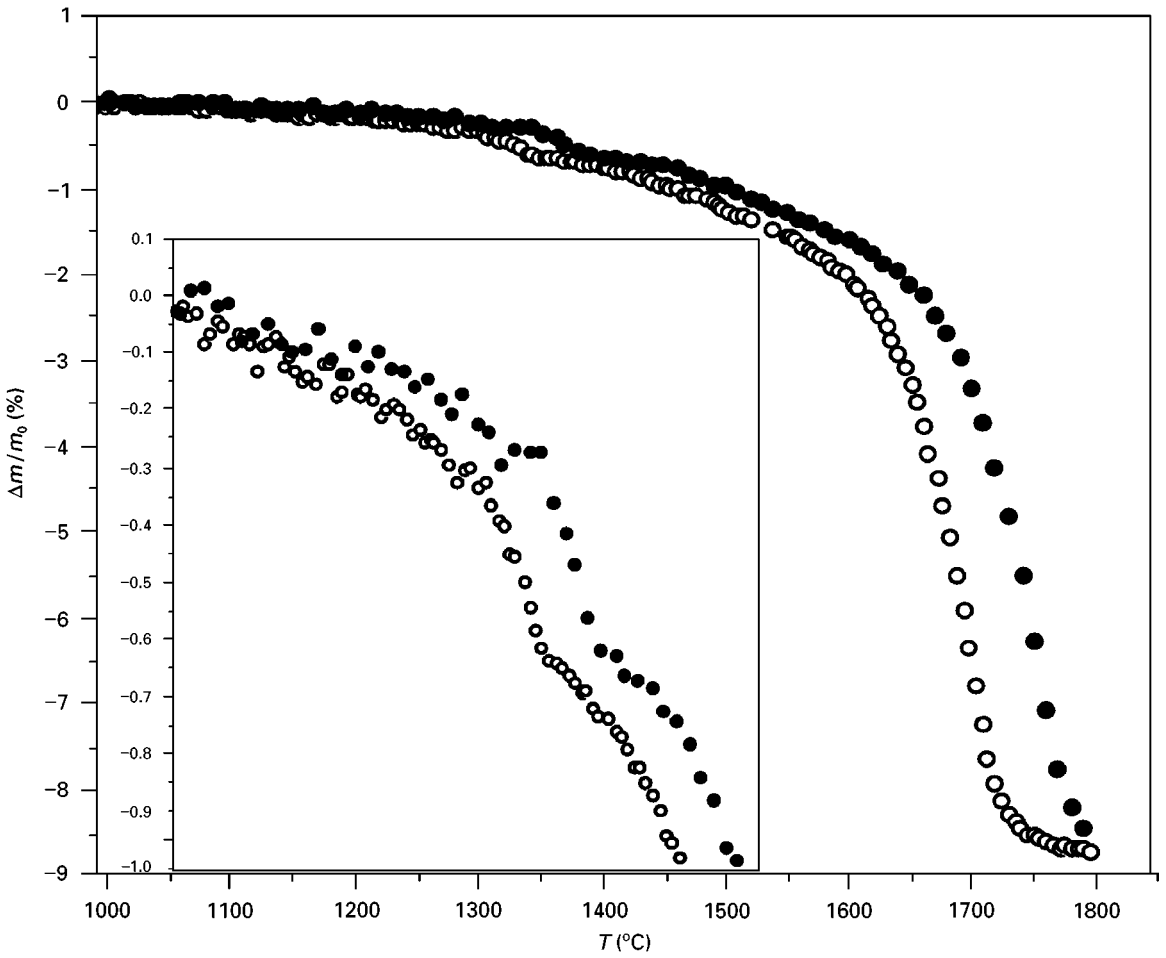

Figure 10 TGA in argon (100 kPa) of the Tyranno Lox-E fibre (insert: detail of the curve for low $\Delta m/m_0$ values and $1050 < T < 1550\,^{\circ}C$). Heating rate: (●) 10 °C min^{-1}, (○) 5 °C min^{-1}.

the first slight weight loss as well as for the corresponding densification that both occur within the same temperature range. The higher temperature weight-loss step (1500–1800 °C) is obviously due to decomposition of the oxycarbide phase with the evolution of oxygen-bearing species, $SiO_{(g)}$ and $CO_{(g)}$, from the surface of the fibre for $T_p = 1300$ °C, and finally from the bulk for $T_p \geqslant 1400$–1600 °C.

3.2. Mechanical properties

3.2.1. Mechanical properties at ambient

The tensile failure strength of the fibre, σ^f, is almost unchanged for $T_p \leqslant 1300$ °C ($t_p = 1$ h) (Fig. 11a). The fracture strength, strongly decreases beyond this temperature (from $T_p = 1350$ °C). For $T_p = 1400$ °C, the retention of strength is only about 25%. The Young's modulus, E, is particularly low for the as-received fibre ($E = 160$ GPa, Fig. 11b). It significantly increases from $T_p = 1100$ to 1300 °C and decreases beyond this temperature. Despite the oxygen-free curing process, the oxygen content is still high enough to induce a drop of the mechanical properties for $T_p \geqslant 1350$ °C. The superficial decomposition of the fibre results in the formation of surface flaws and thus in a drop of failure strength. The low value of the Young's modulus is obviously related to the very low density of the fibre. The presence of an amorphous silicon oxycarbide phase as well as an abundant poorly organized and hydrogenated free-carbon phase lead to low E and ρ values. The increase of E with T_p is an indication of structural evolution of the fibre.

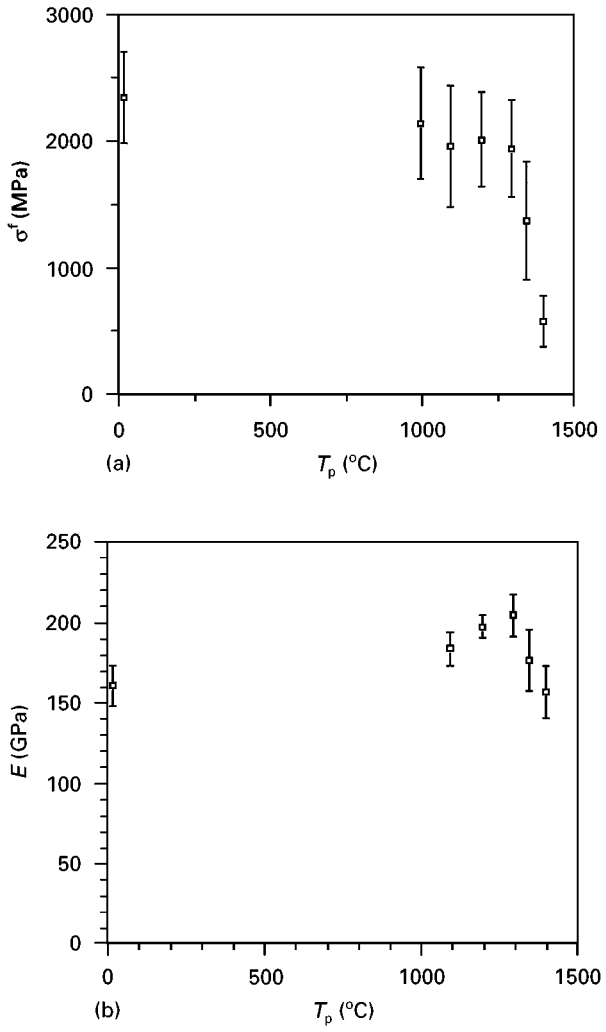

Figure 11 Fracture strength (a) and Young's modulus (b) at ambient of the Tyranno Lox-E fibre versus the annealing temperature, T_p, in argon (100 kPa, $t_p = 1$ h).

3.2.2. Mechanical properties at high temperature

3.2.2.1. Tensile tests. The stress–elongation curves recorded for the fibre at high temperature clearly show a non-elastic behaviour from $T = 1200$ °C that is strongly enhanced as the temperature is raised (Fig. 12). A marked decrease of the stiffness of the fibre is also observed at high temperature. The retention of failure strength is good up to $T = 1200$ °C but rapidly decreases beyond this temperature (Fig. 13).

3.2.2.2. Creep tests. For a given applied stress of 1 GPa, a creep elongation is recorded for $T \geqslant 1100$ °C whose rate is significantly increased with temperature (Fig. 14a). Furthermore the lift-time of the fibre notably decreases with T. It is worthy of note that the Tyranno Lox-E fibre does not exhibit a steady state creep behaviour for $\sigma = 1$ GPa even for the lowest testing temperature. The influence of the applied stress was also studied at $T = 1200$ °C (Fig. 14b). The decrease of the stress results in a decrease of the elongation rate as well as an increase of life-time. An apparent steady state creep domain is observed for $\sigma = 0.5$ GPa. Conversely, for $\sigma = 0.25$ GPa, contraction of the fibre is recorded after transient elongation.

Mechanical tests at high temperature have shown that the fibre exhibits creep deformation at a temperature as low as 1100 °C and a marked viscoelastic behaviour at 1200 °C, which are both thermally activated. This behaviour might be partly due to the presence of the amorphous oxycarbide phase, viscous at high temperature [15–18]. Furthermore, the free carbon phase, which is the major component of the intergranular material, obviously plays a significant role in the origin of creep [27, 38]. The low thermal stability of the fibre that has been established has to be considered. The effects of the structural evolution during the creep test, which are due to thermal instability, are extremely complex to assess. For instance, the absence of a steady state creep-elongation domain and the fibre contraction observed for low applied stress may originate from SiC grain growth [15–16] and the formation of structures and densification of the free carbon phase (simultaneously to hydrogen evolution), i.e. from irreversible thermal effects.

4. Discussion

4.1. For $1000 < T < 1250$–1300 °C

The weak and progressive weight loss observed within this temperature range may be due to an evolution of residual hydrogen from the fibre (this assumption could have been checked by an accurate

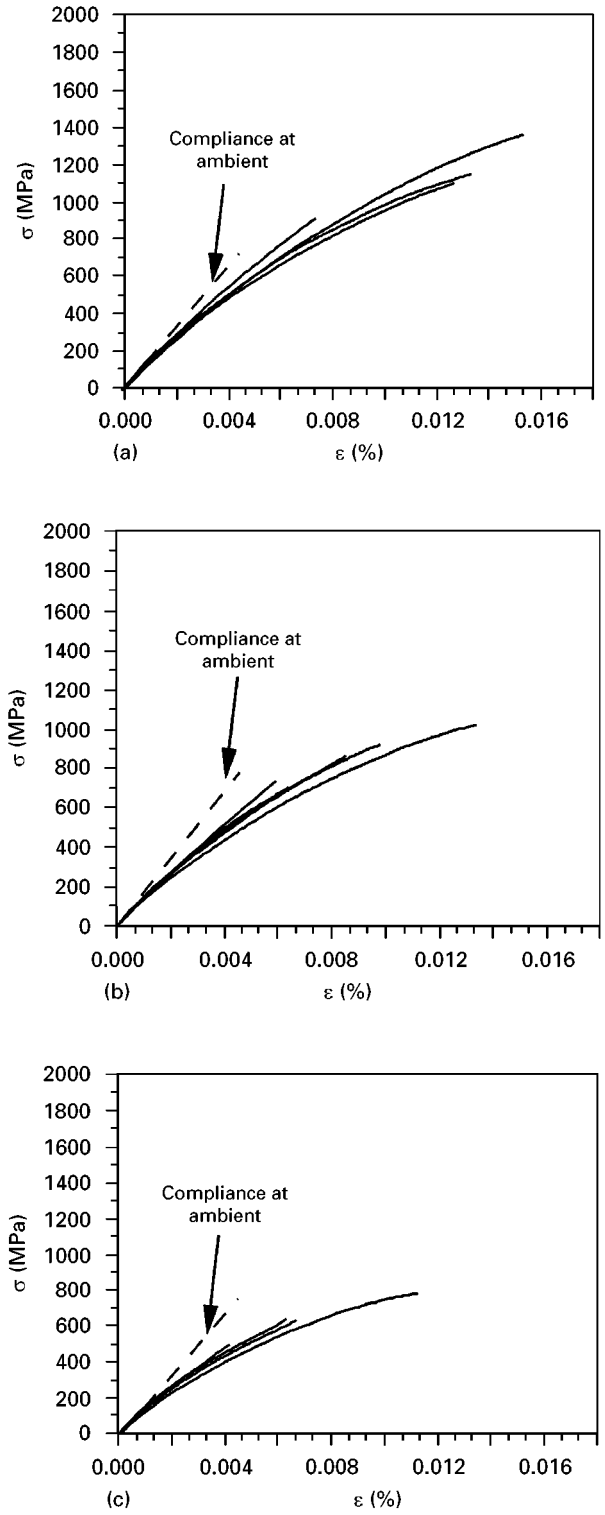

Figure 12 Stress–strain, σ–ε curves of the Tyranno Lox-E fibre in air at high temperature at (a) $T = 1300\,^{\circ}C$, (b) $T = 1350\,^{\circ}C$, and (c) $T = 1400\,^{\circ}C$.

mass spectroscopy analysis). With the exception of the hydrogen concentration, the chemical composition at the surface and in the bulk of the fibre is stable. There is no evolution of SiC grain size up to $T_p = 1200\,^{\circ}C$ ($t_p = 1$ h). This relative structural and chemical stability suggests that the maximum processing temperature is above 1200 °C. The increase of the Young's modulus at ambient observed after annealing at $T_p = 1300\,^{\circ}C$ ($t_p = 1$ h) as well as the densification of the fibre may be due to the dehydrogenation of the free carbon phase and the decrease of nanoporosity.

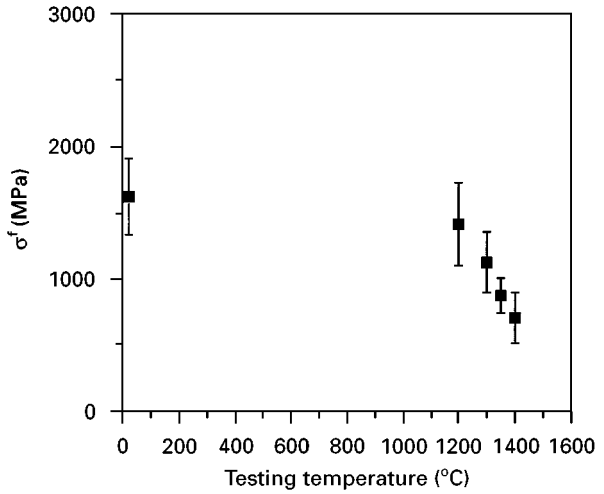

Figure 13 Fracture strength, σ^f, of the Tyranno Lox-E fibre in air at high temperature.

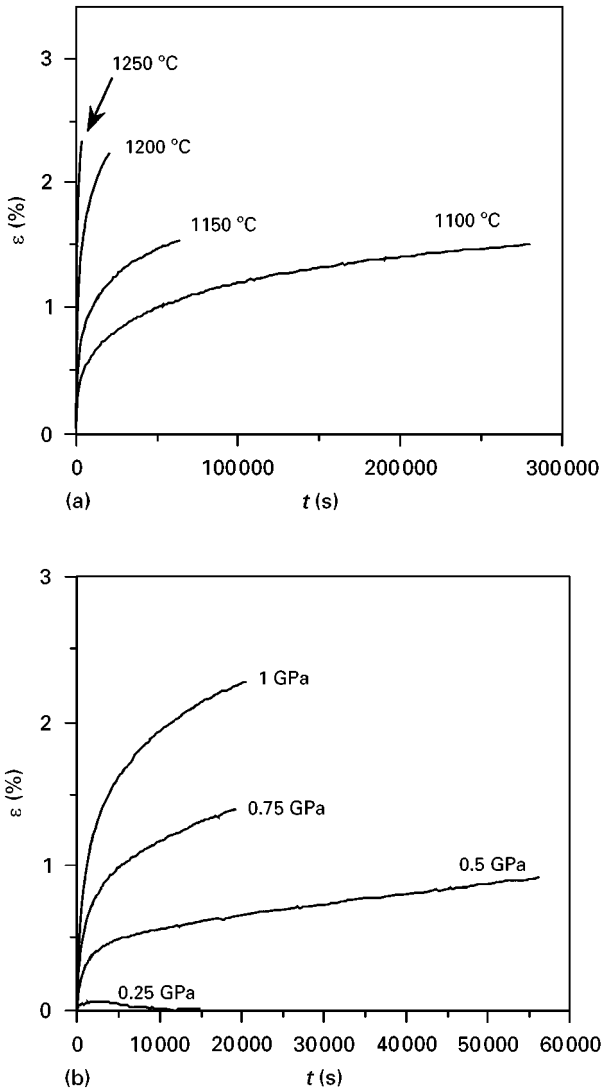

Figure 14 Creep behaviour, ε, in argon of the Tyranno Lox-E fibre versus (a) testing temperature ($\sigma = 1$ GPa) and (b) applied stress ($T = 1200\,^{\circ}C$).

The large decrease of failure strength in air above 1200 °C may originate from the creation of new surface flaws due to the superficial oxidation of the fibre. It could rather be due to the marked viscoelastic

character and the decrease of stiffness of the fibre at this temperature that both decrease the stress level with respect to ambient, for a given magnitude of strain. The catastrophic decrease of the Young's modulus observed beyond 1200 °C can be attributed to the compliant oxycarbide glassy phase but also the poorly organized free carbon phase. The fibres are characterized by a low creep resistance because of the low SiC grain size as well as the presence of abundant viscous (the oxycarbide) and unstable (the free carbon) intergranular phases at high temperature.

4.2. For 1250–1300 < T < 1350–1400 °C

The TGA in argon indicates that this temperature range corresponds first to an increase of the evolution of hydrogen (probably close to the maximum processing temperature) and secondly to the starting decomposition of the oxycarbide phase into $SiO_{(g)}$ and $CO_{(g)}$. The latter feature is confirmed by the vanishing oxygen concentration at 1300 °C (t_p = 1 h). Furthermore, this degradation gives rise to SiC grain coarsening, particularly at the surface of the fibre resulting from the reduction of $SiO_{(g)}$ by free carbon or $CO_{(g)}$. The large surface flaws due to the decomposition–crystallization processes are finally responsible for the large drop of fracture strength observed after annealing at high temperature (T_p = 1350–1400 °C, t_p = 1 h).

4.3. For $T \geqslant$ 1350–1400 °C

The decomposition of the silicon-oxycarbide phase reaches the bulk of the fibre with an apparent "skin–core" texture at T_p = 1600 °C. The SiC grains keep on growing at T_p = 1600 °C (t_p = 1 h) and the weight loss stabilizes at 1800 °C, with complete disappearance of the oxygen from the residues.

5. Conclusions

The present study has shown that the Tyranno Lox-E fibre is chemically and structurally stable in an inert atmosphere (except for the evolution of hydrogen) below 1300 °C. Beyond this temperature, which is probably close to the maximum processing temperature, rapid evolution of the fibre occurs. The decomposition of the silicon oxycarbide first takes place at the surface of the fibre at 1300 °C and then reaches the bulk at higher temperatures. The decomposition yields $SiO_{(g)}$ and $CO_{(g)}$ that react at the surface of the fibre into SiC crystals, resulting in a significant decrease of fracture strength. The low crystal size of the SiC phase as well as the presence of vitreous silicon oxycarbide and a poorly organized free carbon phase at the SiC grain boundary give rise to poor creep resistance of the fibre.

Owing to the relatively high oxygen concentration of the Tyranno Lox-E fibre arising from the PTCS precursor itself, the oxygen-free curing process does not significantly improve the thermal stability of the fibre with respect to the oxygen-cured fibre (Tyranno Lox-E fibre). A new experimental fibre derived from a polyzirconocarbosilane precursor (PZCS) is presently being developed in UBE Industries, which claims to have a lower oxygen content and better thermal resistance.

Acknowledgements

This work has been supported through a grant given by CNRS and the Société Européenne de Propulsion (SEP) to G.C. The authors are indebted to UBE for the supply of the Tyranno Lox-E fibre. They gratefully thank F. Laanani and M. Monthioux from the Laboratoire Marcel Mathieu in Pau for the TEM analyses; Professor A. P. Legrand from Laboratoire de Physique Quantique (ESPCI, Paris) for the NMR analyses; J. Dixmier from Laboratoire Léon Brillouin in Saclay for the neutron diffraction analyses; J. Amiell, A. Marchand and P. Delhaes from the CRPP in Pessac for the ESR analyses; and P. Olry from SEP for valuable discussions.

References

1. S. YAJIMA, J. HAYASHI and M. OMORI, *Chem. Lett.* **9** (1975) 931.
2. S. YAJIMA, K. OKAMURA and J. HAYASHI, *ibid.* **12** (1975) 1209.
3. S. YAJIMA, K. OKAMURA, J. HAYASHI and M. OMORI, *J. Amer. Ceram. Soc. Bull.* **59** (1976) 324.
4. S. YAJIMA, Y. HASEGAWA, J. HAYASHI and M. IIMURA, *J. Mater. Sci.* **13** (1978) 2529.
5. C. LAFFON, A. M. FLANCK, P. LAGARDE, M. LARIDJANI, R. HAGEGE, P. OLRY, J. COTTERET, J. DIXMIER, J. L. MIQUEL, H. HAMMEL and A. P. LEGRAND, *ibid.* **24** (1989) 1503.
6. L. PORTE and A. SARTRE, *ibid.* **24** (1989) 271.
7. P. LE COUSTUMER, M. MONTHIOUX and A. OBERLIN, *J. Eur. Ceram. Soc.* **11** (1993) 95.
8. T. MAH, N. LECHT, D. E. McCULLUM, J. R. HOENIGMAN, H. M. KIM, A. P. KATZ and H. A. LIPSITT, *J. Mater. Sci.* **19** (1984) 1191.
9. T. J. CLARK, R. M. ARONS, I. B. STAMATOFF and J. RABE, *Ceram. Engng Sci. Proc.* **6** [7–8] (1985) 576.
10. S. M. JOHNSON, R. D. BRITTAIN, R. H. LAMOREAU and D. J. ROWCLIFFE, *J. Amer. Ceram. Soc.* **71** (1988) C-132.
11. T. SHIMOO, H. CHEN and K. OKAMURA, *J. Ceram. Soc. Jpn, Int. Edn* **100** (1991) 48.
12. T. J. CLARK, M. JAFFE JR and N. R. LANGLEY, *Ceram. Engng Sci. Proc.* **7** [7–8] (1986) 901.
13. M. H. JASKOWIAK and J. A. DI CARLO, *J. Amer. Ceram. Soc.* **72** (1989) 192.
14. B. A. BENDER, J. S. WALLACE and D. J. SCHRODT, *J. Mater. Sci.* **26** (1991) 970.
15. N. JIA, R. BODET and R. E. TRESSLER, *J. Amer. Ceram. Soc.* **76** (1993) 3051.
16. R. BODET, J. LAMON, N. JIA and R. E. TRESSLER, *ibid.* **79** (1996) 2673.
17. D. J. PYSHER, K. C. GORETTA, R. S. HODDER JR and R. E. TRESSLER, *ibid.* **72** (1989) 284.
18. J. A. DI CARLO, *Comp. Sci. Technol.* **51** (1994) 213.
19. W. TOREKI, C. D. BATICH, M. D. SACKS, M. SALEEM, G. J. CHOI and A. A. MORONNE, *ibid.* **51** (1994) 145.
20. Y. HASEGAWA, *ibid.* **51** (1994) 161.
21. D. C. DELEEUW and J. LIPOWITZ, Eur. Patent 0 438 117 A1, January (1991).
22. M. TAKEDA, Y. IMAI, H. ICHIKAWA, T. ICHIKAWA, T. SEGUSHI and K. OKAMURA, *Ceram. Engng Sci. Proc.* **12** (1991) 1007.

23. M. TAKEDA, Y. IMAI, H. ICHIKAWA, T. ICHIKAWA, N. KASAI, T. SEGUSHI and K. OKAMURA, *ibid.* **13** (1992) 209.
24. *Idem*, *ibid.* **14** (1993) 540.
25. T. YAMAMURA, "Tyranno Fibres", EACM, ECCM-6, Euro–Japanese Colloquium on Ceramic Fibres, Japan Society for Computer Materials, edited by A. R. Bunsell and I. Kimpara, Bordeaux, 23–24 September 1993.
26. J. F. VILLENEUVE, D. MOCAER, R. PAILLER, R. NASLAIN and P. OLRY, *J. Mater. Sci.* **28** (1993) 1227.
27. G. CHOLLON, R. PAILLER, R. NASLAIN and P. OLRY, *ibid.* **32** (1997) 1133.
28. E. BOUILLON, D. MOCAER, J. F. VILLENEUVE, R. PAILLER, R. NASLAIN, M. MONTHIOUX, A. OBERLIN, C. GUIMON and G. PFISTER-GUILLOUZO, *ibid.* **26** (1991) 1517.
29. D. MOCAER, R. PAILLER, R. NASLAIN, C. RICHARD, J. P. PILLOT, J. DUNOGUES, O. DELVERDIER and M. MONTHIOUX, *ibid.* **28** (1993) 2639.
30. F. BELKESSAM LAANANI, PhD thesis, University Paul Sabatier, Touloune (1997).
31. G. CHOLLON, C. LAPORTE, R. PAILLER, R. NASLAIN, F. LAANANI, M. MONTHIOUX and P. OLRY, *J. Mater. Sci.* **32** (1997) 327.
32. J. DIXMIER, "Céramiques à base Si–C–N à partir de précurseurs organosiliciés", Internal Report, Laboratoire de Physique des Solides, Meudon (1991).
33. O. CHAUVET, L. ZUPPIROLI and I. SOLOMON, *Mater. Sci. Engng* **B11** (1992) 303.
34. P. DELHAES and F. CARMONA, Chemistry and Physics of Carbon, edited by P. Thrower **17** (Elsevier, NY, 1981) 89.
35. F. CARMONA, P. DELHAES, G. KERYER and J. P. MANCEAU, *Solid State Commun.* **14** (1974) 1183.
36. C. GERARDIN, PhD thesis, University of Paris VI, Paris (1991).
37. C. GERARDIN, M. HENRY and F. TAULELLE, *Mater. Res. Soc. Symp. Proc.*, edited by M. J. Hampden, W. G. Klemperer and C. J. Brückner, **271** (MRS, San Francisco, CA, 1992) 243.
38. R. BODET, X. BOURRAT, J. LAMON and R. NASLAIN, *J. Mater. Sci.* **30** (1995) 661.

Received 10 March
and accepted 1 September 1997